A correction algorithm to simultaneously control dual deformable mirrors in a woofer-tweeter adaptive optics system

Chaohong Li,[1,2] Nripun Sredar,[1] Kevin M. Ivers,[1] Hope Queener,[1] and Jason Porter[1,3]

[1]*College of Optometry, University of Houston, 505 J. Davis Armistead Bldg., Houston, TX 77204-2020, USA*
[2]*aoeight@hotmail.com*
[3]*jporter@optometry.uh.edu*

Abstract: We present a direct slope-based correction algorithm to simultaneously control two deformable mirrors (DMs) in a woofer-tweeter adaptive optics system. A global response matrix was derived from the response matrices of each deformable mirror and the voltages for both deformable mirrors were calculated simultaneously. This control algorithm was tested and compared with a 2-step sequential control method in five normal human eyes using an adaptive optics scanning laser ophthalmoscope. The mean residual total root-mean-square (RMS) wavefront errors across subjects after adaptive optics (AO) correction were 0.128 ± 0.025 μm and 0.107 ± 0.033 μm for simultaneous and 2-step control, respectively (7.75-mm pupil). The mean intensity of reflectance images acquired after AO convergence was slightly higher for 2-step control. Radially-averaged power spectra calculated from registered reflectance images were nearly identical for all subjects using simultaneous or 2-step control. The correction performance of our new simultaneous dual DM control algorithm is comparable to 2-step control, but is more efficient. This method can be applied to any woofer-tweeter AO system.

OCIS codes: (000.3860) Mathematical methods in physics; (010.1080) Active or Adaptive optics; (330.4460) Ophthalmic optics

References and links

1. J. Liang, D. R. Williams, and D. T. Miller, "Supernormal vision and high-resolution retinal imaging through adaptive optics," J. Opt. Soc. Am. A **14**(11), 2884–2892 (1997).
2. A. Roorda, F. Romero-Borja, W. Donnelly Iii, H. Queener, T. J. Hebert, and M. C. W. Campbell, "Adaptive optics scanning laser ophthalmoscopy," Opt. Express **10**(9), 405–412 (2002).
3. G. Y. Yoon, and D. R. Williams, "Visual performance after correcting the monochromatic and chromatic aberrations of the eye," J. Opt. Soc. Am. A **19**(2), 266–275 (2002).
4. E. A. Rossi, P. Weiser, J. Tarrant, and A. Roorda, "Visual performance in emmetropia and low myopia after correction of high-order aberrations," J. Vis. **7**(8), 14 (2007).
5. E. J. Fernández, P. M. Prieto, and P. Artal, "Binocular adaptive optics visual simulator," Opt. Lett. **34**(17), 2628–2630 (2009).
6. E. Gambra, L. Sawides, C. Dorronsoro, and S. Marcos, "Accommodative lag and fluctuations when optical aberrations are manipulated," J. Vis. **9**(6), 4 (2009).
7. D. C. Gray, W. Merigan, J. I. Wolfing, B. P. Gee, J. Porter, A. Dubra, T. H. Twietmeyer, K. Ahamd, R. Tumbar, F. Reinholz, and D. R. Williams, "In vivo fluorescence imaging of primate retinal ganglion cells and retinal pigment epithelial cells," Opt. Express **14**(16), 7144–7158 (2006).
8. Z. Zhong, B. L. Petrig, X. Qi, and S. A. Burns, "In vivo measurement of erythrocyte velocity and retinal blood flow using adaptive optics scanning laser ophthalmoscopy," Opt. Express **16**(17), 12746–12756 (2008).
9. R. J. Zawadzki, S. S. Choi, A. R. Fuller, J. W. Evans, B. Hamann, and J. S. Werner, "Cellular resolution volumetric in vivo retinal imaging with adaptive optics-optical coherence tomography," Opt. Express **17**(5), 4084–4094 (2009).
10. C. Torti, B. Povazay, B. Hofer, A. Unterhuber, J. Carroll, P. K. Ahnelt, and W. Drexler, "Adaptive optics optical coherence tomography at 120,000 depth scans/s for non-invasive cellular phenotyping of the living human retina," Opt. Express **17**(22), 19382–19400 (2009).
11. R. S. Jonnal, J. R. Besecker, J. C. Derby, O. P. Kocaoglu, B. Cense, W. Gao, Q. Wang, and D. T. Miller, "Imaging outer segment renewal in living human cone photoreceptors," Opt. Express **18**(5), 5257–5270 (2010).

#127858 - $15.00 USD Received 3 May 2010; revised 8 Jul 2010; accepted 17 Jul 2010; published 23 Jul 2010

12. R. A. Applegate, and H. C. Howland, "Magnification and visual acuity in refractive surgery," Arch. Ophthalmol. **111**(10), 1335–1342 (1993).
13. T. Y. Chui, H. Song, and S. A. Burns, "Individual variations in human cone photoreceptor packing density: variations with refractive error," Invest. Ophthalmol. Vis. Sci. **49**(10), 4679–4687 (2008).
14. D. C. Chen, S. M. Jones, D. A. Silva, and S. S. Olivier, "High-resolution adaptive optics scanning laser ophthalmoscope with dual deformable mirrors," J. Opt. Soc. Am. A **24**(5), 1305–1312 (2007).
15. B. Cense, E. Koperda, J. M. Brown, O. P. Kocaoglu, W. Gao, R. S. Jonnal, and D. T. Miller, "Volumetric retinal imaging with ultrahigh-resolution spectral-domain optical coherence tomography and adaptive optics using two broadband light sources," Opt. Express **17**(5), 4095–4111 (2009).
16. R. J. Zawadzki, B. Cense, Y. Zhang, S. S. Choi, D. T. Miller, and J. S. Werner, "Ultrahigh-resolution optical coherence tomography with monochromatic and chromatic aberration correction," Opt. Express **16**(11), 8126–8143 (2008).
17. R. J. Zawadzki, S. S. Choi, S. M. Jones, S. S. Oliver, and J. S. Werner, "Adaptive optics-optical coherence tomography: optimizing visualization of microscopic retinal structures in three dimensions," J. Opt. Soc. Am. A **24**(5), 1373–1383 (2007).
18. J. W. Evans, R. J. Zawadzki, S. M. Jones, S. S. Olivier, and J. S. Werner, "Error budget analysis for an adaptive optics optical coherence tomography system," Opt. Express **17**(16), 13768–13784 (2009).
19. W. Zou, X. Qi, and S. A. Burns, "Wavefront-aberration sorting and correction for a dual-deformable-mirror adaptive-optics system," Opt. Lett. **33**(22), 2602–2604 (2008).
20. W. Zou, and S. A. Burns, "High-accuracy wavefront control for retinal imaging with Adaptive-Influence-Matrix Adaptive Optics," Opt. Express **17**(22), 20167–20177 (2009).
21. S. Hu, B. Xu, X. Zhang, J. Hou, J. Wu, and W. Jiang, "Double-deformable-mirror adaptive optics system for phase compensation," Appl. Opt. **45**(12), 2638–2642 (2006).
22. M. C. Roggemann, and D. J. Lee, "Two-deformable-mirror concept for correcting scintillation effects in laser beam projection through the turbulent atmosphere," Appl. Opt. **37**(21), 4577–4585 (1998).
23. R. Conan, C. Bradley, P. Hampton, O. Keskin, A. Hilton, and C. Blain, "Distributed modal command for a two-deformable-mirror adaptive optics system," Appl. Opt. **46**(20), 4329–4340 (2007).
24. G. Liu, H. Yang, C. Rao, Y. Zhang, and W. Jiang, "Experimental verification of combinational-deformable-mirror for phase correction," Chin. Opt. Lett. **5**, 559–562 (2007).
25. W. Jiang, and H. Li, "Hartmann-Shack wavefront sensing and wavefront control" Proc. SPIE 1271, 82:93 (1990).
26. X. Li, C. Wang, H. Xian, X. Wu, and W. Jiang, "Zernike modal compensation analysis for an adaptive optics system using direct-gradient wavefront reconstruction algorithm," Proc. SPIE **3762**, 116–124 (1999).
27. W. Jiang, Y. Zhang, H. Xian, C. Guan, and N. Ling, "A wavefront correction system for inertial confinement fusion," Proc. of the Second International Workshop on Adaptive Optics for Industry and Medicine pages 8–15, (2000).
28. W. H. Press, S. A. Teukolsky, W. T. Vetterling, and B. P. Flannery, Numerical recipes in C: The art of scientific computing (Cambridge University Press, Cambridge, United Kingdom, 2nd edition, 1992).
29. ANSI, American National Standard for safe use of lasers (ANSI 136.1–2000) (The Laser Institute of America, 2000).
30. F. C. Delori, R. H. Webb, D. H. Sliney; American National Standards Institute, "Maximum permissible exposures for ocular safety (ANSI 2000), with emphasis on ophthalmic devices," J. Opt. Soc. Am. A **24**(5), 1250–1265 (2007).
31. ANSI, American National Standard for ophthalmics-Methods for reporting optical aberrations of eyes (ANSI Z80.28–2004) (American National Standards Institute, Inc., 2004).
32. H. Hofer, L. Chen, G. Y. Yoon, B. Singer, Y. Yamauchi, and D. R. Williams, "Improvement in retinal image quality with dynamic correction of the eye's aberrations," Opt. Express **8**(11), 631–643 (2001).

1. Introduction

Adaptive optics (AO) systems are being used with increased frequency to manipulate the eye's monochromatic aberrations and perform visual psychophysics or conduct high-resolution retinal imaging *in vivo* [1–11]. Traditionally, most deformable mirrors (DMs) used in vision science AO systems possess small magnitudes of stroke and are capable only of correcting higher order aberrations in the majority of eyes. Consequently, trial lenses are often used to correct for the eye's large defocus and astigmatic errors or change the plane of focus within the eye (particularly in small eyes, such as rodents). While these systems have produced excellent retinal images and psychophysical results, it can often be undesirable to use trial lenses to correct lower order aberrations. Back-reflections induced after inserting the trial lens into the optical system can sometimes create havoc with wavefront sensor measurements. Additionally, if a trial lens is positioned immediately in front of the eye (as opposed to being placed exactly in a pupil-conjugate plane), one must account for changes in magnification of the retinal image due to the associated vertex distance [12,13]. To achieve sufficient retinal image quality, one may also need to increase the power of the light entering

#127858 - $15.00 USD Received 3 May 2010; revised 8 Jul 2010; accepted 17 Jul 2010; published 23 Jul 2010

the eye due to light losses introduced by reflections at each surface of the lens for both in-going and out-going light.

With continued developments in large stroke deformable mirror technology, vision scientists are now exploring the use of dual deformable mirror systems to fully correct for the eye's lower and higher order aberrations [14–19]. One such approach, implemented in astronomy and vision science [14–21], is the use of a high-stroke deformable mirror (i.e., woofer) to correct for large amplitude, lower order aberrations and a lower-stroke deformable mirror (i.e., tweeter) to compensate for lower amplitude, higher order aberrations. In vision science, the woofer could compensate for the large individual differences in defocus and astigmatism across eyes, potentially obviating the need for trial lenses. Additionally, the woofer's increased stroke could more easily allow for optical sectioning throughout the entire extent of the retina, as well as correcting fluctuations in accommodation when imaging or psychophysically testing non-cyclopleged eyes.

Several methods have been investigated for controlling dual deformable mirror AO systems, including Zernike modal reconstruction [21], modal decomposition [22,23], zonal reconstruction [19,23,24], and Adaptive Influence Matrix [20] algorithms. These algorithms have been applied in sequential (i.e., an initial woofer correction, followed by a separate tweeter correction) and simultaneous fashions. The direct slope algorithm is a direct and flexible technique that attempts to correct the wavefront by zeroing the local slope vector across the pupil [25]. Despite its prevalent use in single deformable mirror systems, it has been challenging to implement this method in dual deformable mirror systems due to coupling between the woofer and tweeter response matrices. In this paper, we present a direct slope reconstruction algorithm for controlling two deformable mirrors simultaneously. Global response and control matrices are derived for a woofer-tweeter system in which the response matrices for the woofer and tweeter are orthogonal to each other. The correction performance of this simultaneous control algorithm was compared to a 2-step (or sequential) control method in normal human eyes and found to yield similar retinal image quality and residual levels of aberration after correction.

2. Theory of direct slope-based simultaneous control algorithm for a dual DM system

2.1. Removal of coupling between woofer and tweeter

To efficiently operate a woofer-tweeter system using a direct slope-based algorithm, it is important to remove any coupling between the woofer and tweeter response matrices and prevent both deformable mirrors from producing piston, tip and tilt. The direct slope algorithm for a single deformable mirror AO system stipulates that the slope vector (S) obtained from the n_s slope measurements acquired by the wavefront sensor be equal to a linear combination of the deformable mirror's response matrix (D) and actuator voltage command vector (V) [25–27]:

$$S = DV \tag{1}$$

To generate an algorithm that simultaneously controls two deformable mirrors, we first assume that the tweeter contains a higher number of actuators (n_t actuators) than the woofer (n_w actuators) over the effective pupil. Next, we construct a new response matrix for the tweeter (D_t') that is orthogonal to the woofer's response matrix (D_w). The tweeter's new response matrix is made by subtracting D_{tw}, the projection of the tweeter's original response matrix (D_t) onto the woofer's response matrix, from the tweeter's original response matrix:

$$D_t' = D_t - D_{tw} \tag{2}$$

D_{tw} is given by

$$D_{tw} = D_w C_{tw} \tag{3}$$

where C_{tw} is a matrix containing the coefficients resulting from the projection of the tweeter's original response matrix onto the woofer's response matrix. This coefficient matrix can be

#127858 - $15.00 USD Received 3 May 2010; revised 8 Jul 2010; accepted 17 Jul 2010; published 23 Jul 2010

determined by applying the classic direct slope algorithm [Eq. (1)] to the woofer and the tweeter independently:

$$\begin{aligned} S &= D_t V_t \\ S &= D_w V_w \end{aligned} \tag{4}$$

where V_w and V_t are the voltage vectors for the woofer and tweeter, respectively. Using singular value decomposition, we can solve for V_w and determine the coupling between the woofer and the tweeter:

$$\begin{aligned} V_w &= D_w^{\dagger} S \\ &= D_w^{\dagger} D_t V_t \\ &= C_{tw} V_t \end{aligned} \tag{5}$$

where $D_w^{\dagger}$ is the pseudo-inverse matrix of the woofer's response matrix. Substituting C_{tw} into Eq. (2) and (3), we find the new tweeter response matrix which is now orthogonal to the woofer's response matrix:

$$D_t' = D_t - D_w C_{tw} = D_t - D_w (D_w^{\dagger} D_t) \tag{6}$$

2.2. Removal of piston, tip, and tilt

To minimize the likelihood that each deformable mirror will produce piston, we must ensure that the sum of the voltages applied to all actuators is zero for the woofer and the tweeter:

$$\sum_{i=1}^{n_w} V_{w,i} = \sum_{i=1}^{n_t} V_{t,i} = 0 \tag{7}$$

Similarly, to minimize the likelihood of producing tip and tilt in each deformable mirror, the sum of the inner product of each actuator's position vector and the corresponding voltage applied at that actuator must be zero:

$$\begin{aligned} \sum_{i=1}^{n_w} X_i V_{w,i} &= \sum_{i=1}^{n_w} Y_i V_{w,i} = 0 \\ \sum_{i=1}^{n_t} X_i V_{t,i} &= \sum_{i=1}^{n_t} Y_i V_{t,i} = 0 \end{aligned} \tag{8}$$

where X_i and Y_i are the x- and y-positions of each actuator defined in the unit circle. In matrix form, Eq. (7) and (8) may be written as

$$\begin{bmatrix} 1 & \dots & 1 \\ X_1 & \dots & X_{n_w} \\ Y_1 & \dots & Y_{n_w} \end{bmatrix} \begin{bmatrix} V_{w,1} \\ \dots \\ V_{w,n_w} \end{bmatrix} = C_w V_w = 0 \text{ and } \begin{bmatrix} 1 & \dots & 1 \\ X_1 & \dots & X_{n_t} \\ Y_1 & \dots & Y_{n_t} \end{bmatrix} \begin{bmatrix} V_{t,1} \\ \dots \\ V_{t,n_t} \end{bmatrix} = C_t V_t = 0 \tag{9}$$

The new global response matrix for the woofer-tweeter system, D_{wt}, can be written as

$$D_{wt} = \begin{bmatrix} D_w & D_t' \\ C_w & 0 \\ 0 & C_t \end{bmatrix} \tag{10}$$

where the last two rows include the constraints illustrated in Eq. (9) to zero piston, tip and tilt. Matrix D_{wt} contains $(n_s + 6)$ rows and $(n_w + n_t)$ columns. The number of rows is given by the sum of the rows in matrices D_w and D_t' (n_s rows), C_w (3 rows), and C_t (3 rows). The number of columns is given by the sum of the columns in matrices D_w and C_w (n_w columns), and D_t' and C_t (n_t columns).

The new slope vector for the dual deformable mirror system (based on the direct slope algorithm) can be expressed as

#127858 - $15.00 USD Received 3 May 2010; revised 8 Jul 2010; accepted 17 Jul 2010; published 23 Jul 2010

$$S = D_{wt}V_{wt} = \begin{bmatrix} D_w & D_t' \\ C_w & 0 \\ 0 & C_t \end{bmatrix} \begin{bmatrix} V_w \\ V_t \end{bmatrix} = D_w V_w + D_t' V_t \quad (11)$$

The global control matrix can be obtained by applying singular value decomposition to the global response matrix, D_{wt}, in Eq. (11) [28]. Notice that the dimensions for the pseudo-inverse matrix of D_{wt} should be $(n_w + n_t) \times (n_s + 6)$. The global control matrix can be obtained by extracting a subset of the pseudo-inverse matrix of D_{wt} of dimensions $(n_w + n_t) \times n_s$. We can calculate the voltages to simultaneously apply to the woofer and tweeter via

$$[V_w; V_t] = D_{wt}^{\dagger}{}_{[1:(n_w+n_t),1:n_s]} S \quad (12)$$

3. Methods

3.1. Woofer-tweeter adaptive optics scanning laser ophthalmoscope

The performance of the direct slope-based algorithm for simultaneously controlling two DMs was tested using a woofer-tweeter adaptive optics scanning laser ophthalmoscope (AOSLO). The AOSLO [shown in Fig. 1(a)] consists of a Shack-Hartmann wavefront sensor (SHWS), a woofer (Mirao 52-e, Imagine Eyes, Inc., France), a tweeter (Multi-DM MEMS mirror, Boston Micromachines Inc., Cambridge, MA), an imaging light source, and a detector to accommodate for near-infrared reflectance imaging. A superluminescent diode (Superlum, Ireland) with a center wavelength of 840 nm is used for wavefront sensing and reflectance imaging. Light from the superluminescent diode (SLD) is raster scanned across the retina using a resonant scanner (Electro-Optical Products Corp, Glendale, NY) driven sinusoidally at 14.62 kHz to provide the horizontal scan and a galvanometric scanner (GSI Group Corp, Bedford, MA) driven in a saw-tooth pattern at 25 Hz to provide the vertical scan. The scan angle is adjustable to a maximum field size of 3 degrees.

Approximately 20% of the light that reflects from the retina and propagates back through the system is diverted to the wavefront sensor while the residual light is transmitted to a photomultiplier tube (PMT) for retinal imaging. Wavefront sensing and AO correction are performed over a maximum pupil size of 8 mm (at the plane of the eye) at a rate of 9-11 Hz. The SHWS consists of a lenslet array with a 300-μm lenslet diameter and a 7.6-mm focal length. The effective pupil diameter at the lenslet array is 4.9 mm and incorporates 208 subapertures (16 x 16 array). The woofer (Mirao 52-e) was placed between the scanners and the eye [15] and has a total of 52 actuators with a spacing of 2.5 mm, a maximum wavefront stroke of 50 μm and a measured inter-actuator coupling of 0.60. The tweeter (MEMS) has a total of 140 acutators with a spacing of 450 μm, a maximum wavefront stroke of 5.5 μm and an inter-actuator coupling of 0.32. The effective beam diameters on the woofer and tweeter were 13.2 mm (incorporating 32 actuators) and 4.9 mm (incorporating 120 actuators), respectively. Figure 1(b) shows the geometry and spatial relationship of the Shack-Hartmann lenslets and woofer and tweeter actuators.

Reflectance retinal images were acquired by the PMT at a rate of 25 Hz. A confocal pinhole with a diameter of ~1.5 Airy disk diameters (75 μm) was placed in front of the PMT at a retinal conjugate plane. Registered images were generated by cross-correlating and averaging multiple frames to remove the deleterious effects of eye movements and increase the signal-to-noise ratio of the retinal images.

#127858 - $15.00 USD Received 3 May 2010; revised 8 Jul 2010; accepted 17 Jul 2010; published 23 Jul 2010

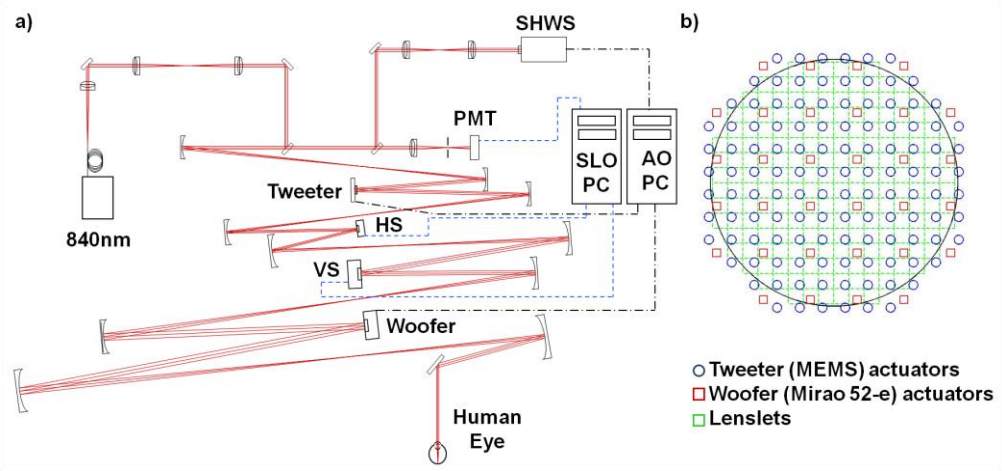

Fig. 1. (a) The woofer-tweeter adaptive optics scanning laser ophthalmoscope (AOSLO). 840nm: SLD with center wavelength of 840 nm, Tweeter: BMC MEMS deformable mirror, HS: horizontal scanner (14.62 kHz), VS: vertical scanner (25 Hz), Woofer: Mirao-52e deformable mirror, SHWS: Shack-Hartmann wavefront sensor, PMT: photomultiplier tube for near-infrared reflectance imaging. (b) Spatial geometry of the Shack-Hartmann lenslets (green squares), tweeter actuators (blue circles), and woofer actuators (red squares) in the pupil plane.

3.2. Subjects

The performance of the control algorithm was tested in five human subjects that ranged in age between 25 and 35 years. The manifest spherical and cylindrical refractive errors ranged from 0.00 to −3.25 Diopters (D) and 0.00 to −1.25 D, respectively. Informed consent was obtained from each subject prior to being enrolled in the study in accordance with the Declaration of Helsinki.

3.3. Experimental comparison of AO control methods

Subjects were dilated with 1 drop of 2.5% phenylephrine and 1 drop of 1% tropicamide. No subjects wore their best correction nor was there any pre-compensation of defocus and astigmatism prior to AO correction. Consequently, we were not able to acquire a full set of Shack-Hartmann spots across the entire dilated pupil before AO correction in all eyes. (This is due to the fact that moderate to large amounts of defocus in the Shack-Hartmann spot pattern lead to a reduced number of spots initially in these eyes. As adaptive optics corrects the eye's defocus (and higher order aberrations), the number of Shack-Hartmann spots will increase until the maximum number of spots corresponding to the subject's dilated pupil has been obtained.) Therefore, after full dilation was achieved, we measured each subject's native, total wave aberration over their maximum pupil diameter using a COAS-HD wavefront sensor (AMO WaveFront Sciences, Albuquerque, NM).

A bite bar was used to stabilize each subject's head while subjects fixated the top right corner of the raster pattern at an eccentricity of ~1°. The power of the 840 nm SLD at the corneal plane was ~295 μW which was greater than 10 times below the maximum permissible exposure (MPE) for a 1.5° field size and a 1.5 hour exposure time (according to the ANSI guide for the safe use of lasers [29] and the "translation" of the ANSI standard for typical devices by Delori et al. [30]). Prior to testing the dual DM control algorithms, the response matrices were measured separately for the woofer and the tweeter based on the traditional direct slope control algorithm for a single DM.

Using the AOSLO, we simultaneously initiated the recording of Shack-Hartmann wavefront sensor spot array images and reflectance retinal images (1.5° field) as aberrations were corrected using one of the following methods: (a) woofer only control, (b) 2-step sequential control (i.e., woofer correction first followed by a separate tweeter correction), or

#127858 - $15.00 USD Received 3 May 2010; revised 8 Jul 2010; accepted 17 Jul 2010; published 23 Jul 2010

(c) simultaneous dual DM control based on the woofer-tweeter direct slope algorithm. Frames were captured for each subject over at least 25 seconds. Five trials were conducted randomly for each correction method using a constant proportional integral gain control of 0.5.

Pupil plane and image plane metrics were examined to assess the performance of each control method. The mean Shack-Hartmann spot displacement (i.e., the mean magnitude of the vector displacement of each lenslet's centroid position from its reference position) was calculated for each frame in the series of Shack-Hartmann spot array images acquired using each control method. Additionally, the residual total and higher order root-mean-square (RMS) wavefront errors were calculated after the AO correction had converged for the largest dilated pupil size common to all subjects. (Total aberrations included Zernike polynomials of the 2nd through 10th radial orders while higher order aberrations included 3rd through 10th radial orders [31].) The impact of each control method on retinal image quality was assessed by calculating the intensity of reflectance frames acquired in each condition and examining the radially-averaged power spectrum of the registered images. Retinal images were scaled from minutes of visual angle to microns on the retina based on axial length measurements acquired in each subject with an IOLMaster (Carl Zeiss Meditec, Inc., Dublin, CA).

4. Results

4.1. Performance comparison in the pupil plane

Table 1 shows the mean RMS wavefront errors for each subject measured before AO correction (using the COAS-HD wavefront sensor) and after AO correction (using the AOSLO's wavefront sensor) for the 2-step and simultaneous dual DM control methods. Aberrations were calculated for a 7.75-mm pupil diameter (corresponding to the largest pupil size common to all subjects). The residual RMS wavefront errors after AO represent the mean errors calculated over the first 80 frames after the correction had converged using the simultaneous and 2-step control methods.

Table 1. Sphere, cylinder, total RMS and higher order RMS wavefront errors before and after AO correction using simultaneous and 2-step dual DM control methods for 5 subjects (7.75-mm pupil)

	Aberrations before AO correction			Aberrations after AO correction	
				Simultaneous correction	2-step correction
Subject	Sphere (D)	Cylinder (D)	Total / Higher order RMS (μm)	Total / Higher order RMS (μm)	Total / Higher order RMS (μm)
1	0.00	–0.50	1.347 0.768	0.116 ± 0.010 0.047 ± 0.004	0.108 ± 0.007 0.027 ± 0.005
2	–0.25	–1.25	2.712 0.953	0.125 ± 0.009 0.052 ± 0.006	0.140 ± 0.015 0.071 ± 0.015
3	–1.50	–1.00	5.008 0.518	0.102 ± 0.006 0.024 ± 0.002	0.051 ± 0.005 0.032 ± 0.002
4	–3.00	–0.75	6.584 0.487	0.176 ± 0.069 0.086 ± 0.047	0.140 ± 0.014 0.097 ± 0.011
5	–3.25	0.00	7.001 0.495	0.119 ± 0.025 0.074 ± 0.007	0.095 ± 0.016 0.065 ± 0.012

As seen in Table 1, the 2-step and simultaneous dual DM control methods considerably reduced the total magnitude of aberration for this large pupil diameter. Both methods of correction produced very similar values of residual RMS wavefront error after AO when compared within individual subjects. The mean magnitude of the difference in residual total RMS wavefront error between simultaneous and 2-step correction across eyes was 0.027 μm while that for residual higher order RMS error was 0.013 μm. In general, the residual total and higher order RMS wavefront errors after correction tended to be higher in subjects with larger magnitudes of total RMS wavefront error prior to correction.

To assess convergence using the three different methods of AO control (i.e., woofer only, 2-step and simultaneous dual DM), the mean Shack-Hartmann spot displacement and the

#127858 - $15.00 USD Received 3 May 2010; revised 8 Jul 2010; accepted 17 Jul 2010; published 23 Jul 2010

mean radius of the normalized Shack-Hartmann pupil were calculated over time for each subject and plotted in Fig. 2. AO correction began at time t = 0 seconds in each diagram. Recall, the 2-step sequential control method requires a woofer only correction, followed by a tweeter only correction. Therefore, the 2-step correction method is represented in Fig. 2 as a combination of the woofer only curve (black solid line) and 2-step (post-woofer) curve (green solid line). The 2-step (post-woofer) curve illustrates the tweeter only component of the 2-step correction method and begins after the woofer has converged. For clarity and ease of comparison, only the mean curves obtained from the 5 trials (with no error bars) are plotted for each control method. Values describing the fluctuations about each mean curve are shown in Table 2 and were calculated as follows. For each control method, an average value for the mean spot displacement (MSD) and its associated standard deviation were calculated across all trials at each time point (excluding any Shack-Hartmann frames in which a blink occurred). The values listed in Table 2 are the mean of these standard deviation values averaged over all time points plotted in Fig. 2 and represent the variability in each mean curve across trials. For example, eyes with larger amounts of lower order aberrations before correction tended to experience more fluctuations in the mean spot displacement and rate of convergence from trial to trial. Consequently, these eyes generally had larger mean standard deviations of the MSD.

Different convergence times were measured for different subjects, largely depending on the amount of total aberration that needed to be corrected. Within a subject, the rate and level of convergence were nearly the same for the 2-step and simultaneous dual DM control algorithms. Some subjects, such as 1 and 2, had low amounts of aberration and were able to be maximally corrected in ≤ 2 seconds with either the 2-step or simultaneous correction methods. Other subjects with increased amounts of total aberration required a longer time to converge to a minimal MSD value. After convergence was achieved, however, the MSD values for all subjects were very similar regardless of the control method (2-step vs. simultaneous) or total amount of aberration prior to correction.

Also, the uncorrected defocus and astigmatism inherent in most subjects' eyes prior to AO correction resulted in a reduced number of detected Shack-Hartmann spots and an effective pupil diameter that was less than the maximum number of spots expected based on the subject's dilated pupil size. Therefore, we calculated a normalized pupil radius over which the Shack-Hartmann spots could be detected throughout the entire correction. As shown in Fig. 2, the normalized pupil radius (dashed lines) over which Shack-Hartmann spots could be sufficiently detected was typically less than 1 at the beginning of the correction and increased to its maximum value of 1 as the AO correction progressed and converged.

#127858 - $15.00 USD Received 3 May 2010; revised 8 Jul 2010; accepted 17 Jul 2010; published 23 Jul 2010

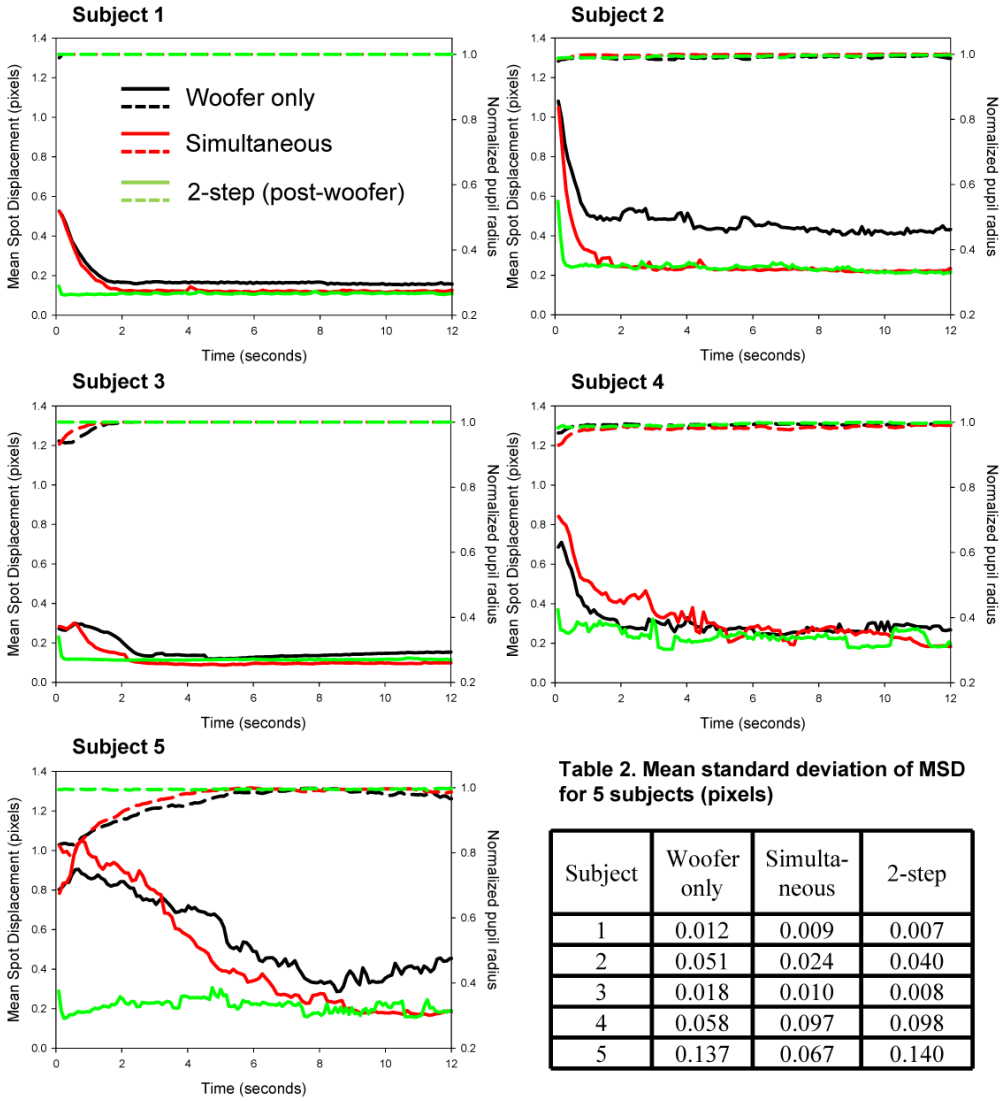

Table 2. Mean standard deviation of MSD for 5 subjects (pixels)

Subject	Woofer only	Simulta-neous	2-step
1	0.012	0.009	0.007
2	0.051	0.024	0.040
3	0.018	0.010	0.008
4	0.058	0.097	0.098
5	0.137	0.067	0.140

Fig. 2. Changes in mean spot displacement (solid lines) and normalized pupil radius (dashed lines) of the Shack-Hartmann wavefront sensor spots as a function of time in 5 subjects for 3 different control methods: woofer only (black), 2-step sequential, and simultaneous (red). The 2-step sequential control method includes two components: woofer only correction (black), followed by the 2-step (post-woofer) correction (green), or tweeter only correction, initiated after the woofer converged. Each curve represents the mean of 5 trials. The mean standard deviation of the mean spot displacement (MSD) is shown in Table 2 and represents the variability inherent in each mean curve. AO correction was initiated at time = 0 seconds. In general, the time to convergence increased in eyes with increasing amounts of aberration. However, the convergence time and the MSD values after convergence were nearly identical for 2-step and simultaneous control within a subject.

4.2. Performance comparison in the retinal image plane

In addition to recording the Shack-Hartmann spot array images, reflectance images of the cone photoreceptor mosaic were acquired in each subject at 1 degree eccentricity during AO correction. We examined the amount of light that was focused through the confocal pinhole (placed in a retinal conjugate plane immediately before the PMT) and detected by the PMT with each method of aberration correction. The mean intensity of each reflectance frame

#127858 - $15.00 USD Received 3 May 2010; revised 8 Jul 2010; accepted 17 Jul 2010; published 23 Jul 2010

(excluding frames in which the subject blinked) was calculated and subsequently averaged over 500 consecutive frames after the correction had converged for each trial. The mean intensity of the reflectance images across trials was calculated for each control method and plotted in Fig. 3 for all subjects. The mean intensity was lowest in all eyes for the woofer only correction and was highest for 2-step sequential control. Simultaneous and 2-step control methods yielded very similar values for most subjects with subjects 4 and 5 displaying the largest differences in mean intensity between methods. Using a one-way repeated measures ANOVA (Analysis of Variance), we found that the mean retinal image intensity obtained using 2-step control was close to being statistically significantly different from the mean retinal image intensity using simultaneous control ($p = 0.05$) across subjects.

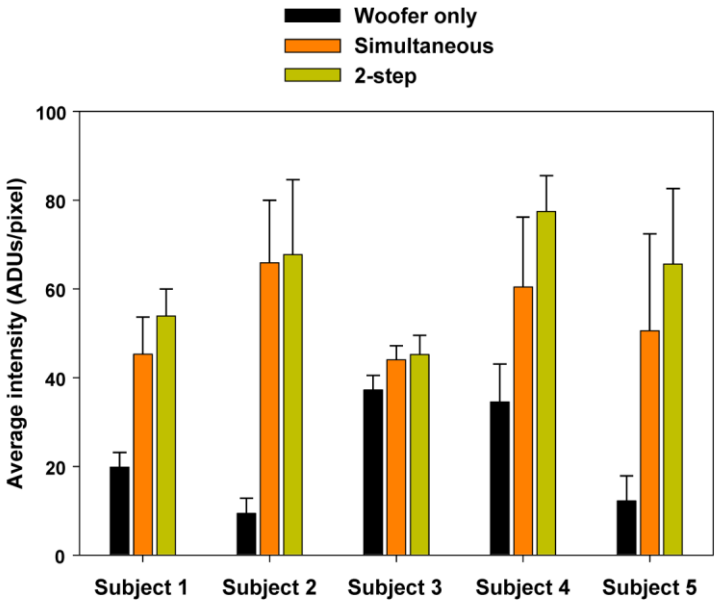

Fig. 3. Average intensity of the retinal reflectance images acquired using different control methods in 5 subjects. Plotted are the mean intensity values averaged over 500 frames acquired for each of 5 trials after AO convergence using the woofer only (black bars), simultaneous dual DM (orange bars) and 2-step sequential (green bars) control methods. Error bars represent ± 1 standard deviation about the mean intensity. The 2-step control method yielded average intensity values that tended to be slightly greater than those obtained from simultaneous control.

To better compare the quality and overall content of the reflectance images, 20 raw reflectance frames were averaged to create a registered image of the cone mosaic for each method of control. Examples of these images are shown in Fig. 4 for the two subjects in our study who possessed the highest magnitude of total RMS wavefront error. Qualitatively, the registered reflectance images acquired using the simultaneous dual DM and 2-step sequential control algorithms were nearly identical for all subjects. We calculated the radial power spectrum density for each registered image to better assess quantitatively any differences in the spatial frequency content of retinal images acquired using the simultaneous and 2-step control methods. The right-most column of Fig. 4 shows the power spectra calculated from the adjacent retinal images that were taken during simultaneous and 2-step AO control in subjects 4 and 5. As shown in the figure, the radial power spectra for each control method were nearly identical, indicating that simultaneous dual DM and 2-step sequential control algorithms yielded similar performance as assessed by direct examination of the retinal image.

#127858 - $15.00 USD Received 3 May 2010; revised 8 Jul 2010; accepted 17 Jul 2010; published 23 Jul 2010

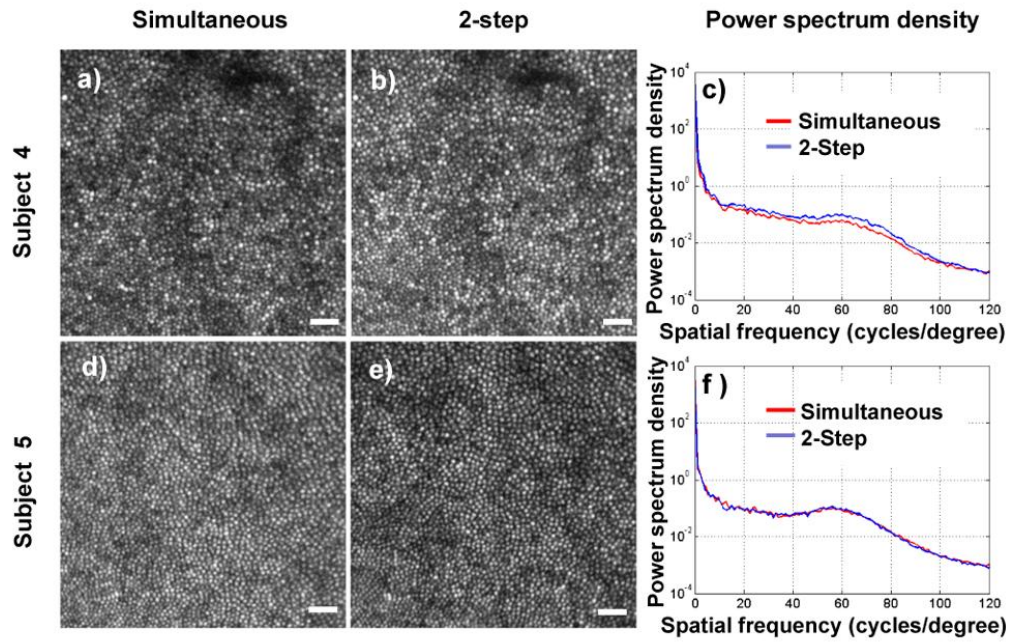

Fig. 4. Registered reflectance images and associated radially-averaged power spectra for two AO control methods in 2 subjects. Registered images of the cone photoreceptor mosaic were constructed from 20 frames acquired after AO convergence using (a,d) simultaneous dual DM and (b,e) 2-step sequential control algorithms. Images were taken at an eccentricity of 1 degree. Scale bar represents 30 microns. Qualitatively, retinal images were very similar across control methods within individual subjects. (c,f) Radially-averaged power spectra (computed from the registered images) for simultaneous control (red line) and 2-step control (blue line) as a function of spatial frequency. The radial power spectra obtained using both control methods are quantitatively similar.

This finding was consistent across subjects and is illustrated in Fig. 5, which plots the ratio of the radial power spectra obtained from retinal images acquired using simultaneous control to that obtained from 2-step control in each subject as a function of spatial frequency. Ratios greater than 1 indicate that the value for the radial power spectrum was greater for simultaneous control at the given spatial frequency while ratios less than 1 indicate that the value for the radial power spectrum was greater for 2-step control at the given spatial frequency. A ratio of 1 indicates both methods yielded the same result. As seen in the figure, the ratio of the radial power spectra in some subjects (e.g., subjects 1, 2 and 4) was less than 1 for most spatial frequencies, indicating slightly better correction using the 2-step control method for these spatial frequencies. However, ratios hovered about 1 or were slightly higher than 1 across most spatial frequencies for other subjects (e.g., subjects 3 and 5), indicating that simultaneous control yielded at least similar correction performance to 2-step control according to the power spectra.

5. Discussion

The primary goals of this paper were to introduce a new direct slope-based algorithm for simultaneously controlling a woofer-tweeter AO system and to compare its correction performance with a 2-step sequential control method in human eyes. In this new direct slope-

#127858 - $15.00 USD Received 3 May 2010; revised 8 Jul 2010; accepted 17 Jul 2010; published 23 Jul 2010

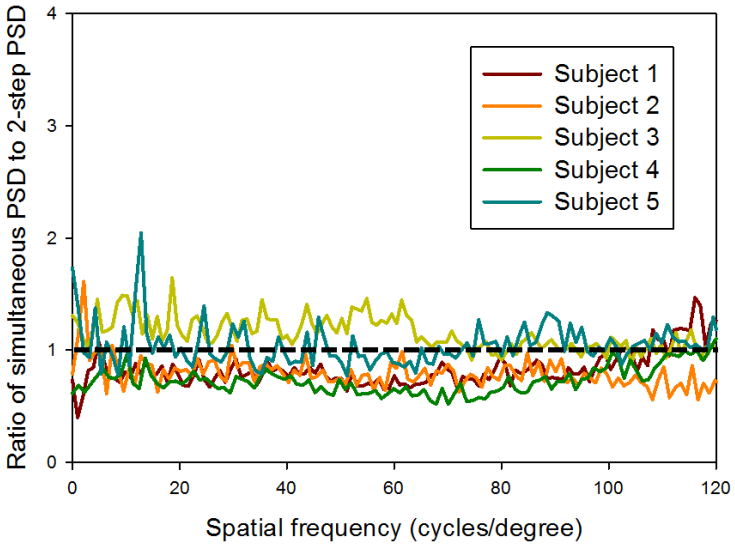

Fig. 5. Ratio of the radial power spectrum density (PSD) obtained from retinal images acquired using simultaneous control to the radial power spectrum density from retinal images acquired using 2-step sequential control in 5 subjects. A ratio of 1 (dashed black line) indicates that the radial power spectrum was identical for each control method. A ratio greater/less than 1 implies that the radial power spectrum was greater for the simultaneous/2-step control method, respectively. Across the majority of spatial frequencies, the ratio hovered around 1, indicating that the radial power spectrum was approximately the same between the two control methods.

based algorithm, a new tweeter response matrix [Eq. (6)] was derived to be orthogonal to the woofer's response matrix and minimize coupling between the woofer and the tweeter. Global response and control matrices were derived for simultaneously controlling the woofer and the tweeter while attempting to minimize the piston, tip and tilt produced by the system. Despite the fact that tip and tilt are not typically corrected in vision science AO systems, this simultaneous dual DM control algorithm could also be used to control a tip-tilt and woofer-tweeter system in other applications (such as astronomy).

The correction performances of woofer only control, 2-step sequential control and simultaneous dual DM control were examined in five normal human eyes. The residual total RMS wavefront errors were nearly identical when using the 2-step and simultaneous dual DM control methods within a subject (Table 1), indicating 2-step sequential and simultaneous dual DM control methods provided similar correction performance. The mean residual total RMS errors were slightly lower in 4 of 5 subjects following AO correction using 2-step sequential control. The mean residual higher order RMS wavefront errors were lower in subjects 2, 3 and 4 after AO correction using simultaneous control.

In addition to comparing RMS wavefront errors after convergence, we also analyzed the mean spot displacements of the Shack-Hartmann spots during correction for each control method. Changes in mean spot displacement were measured instead of changes in RMS wavefront error for several reasons. First, no corrections were implemented to compensate for a subject's sphere and cylinder prior to AO correction. Therefore, it was common for the Shack-Hartmann wavefront sensor to begin AO correction based on a reduced array of spots (i.e., a small effective pupil diameter) that gradually became complete and filled the entire dilated pupil with correction. Since the effective pupil size typically changed during correction, we would have been restricted to calculating the RMS wavefront error over the largest pupil diameter common to all of the Shack-Hartmann frames. This pupil diameter would have been less than each subject's maximum dilated pupil size and would have varied

#127858 - $15.00 USD Received 3 May 2010; revised 8 Jul 2010; accepted 17 Jul 2010; published 23 Jul 2010

from subject to subject. Secondly, calculation of the RMS wavefront error is dependent on first fitting a polynomial (typically a Zernike polynomial) to the measured slope data. Any small errors associated with this fit could add noise to the correction performance assessment. Mean spot displacement, on the other hand, is calculated directly from the raw spot positions in each frame with no fitting required.

The aberration profile of each subject contributed to the time taken for the AO correction to converge. As seen in Fig. 2, the time required for the AOSLO to converge to a stable correction increased, in general, as the magnitude of the subject's sphere and cylinder also increased. The convergence time associated with each method of control was partly limited by the ~10 Hz sampling rate of the Shack-Hartmann wavefront sensor. This low sampling rate was dictated by a host of factors, including the maximum frame rate of our wavefront sensor CCD (~20 Hz full frame with no binning), temporal instabilities in the Mirao 52-e's mirror surface (i.e., woofer) immediately after applying a set of voltages, and the required exposure time (~20 ms) based on our system throughput. If we were able to measure and correct aberrations at a rate of 30 Hz (typically, a maximum rate used by vision science AO systems [32]), it could be possible to achieve convergence times that would be ~3x faster than those measured in this study. Also, it is important to note that the woofer and the tweeter were updated at the same rate when correcting aberrations using simultaneous control. Further studies would be required to investigate the performance of this simultaneous dual DM control method if one wished to control the woofer and the tweeter at different frequencies (as might be done in astronomical applications to achieve faster response times).

While simultaneous control yielded convergence times similar to 2-step sequential control, simultaneous control is actually faster in practice. Two-step sequential control typically requires the user to stop the woofer correction and start the tweeter correction. However, user intervention is not required when using the simultaneous dual DM control method. Even though this benefit may seem trivial, it can be meaningful in different experimental situations. For example, simultaneous control can be advantageous (over 2-step control) when attempting to image patients with poor fixation and/or large eye movements. In these patients, one typically has small windows of time in which to correct aberrations and acquire retinal images or perform visual psychophysics. Correcting aberrations in 1-step as opposed to 2 discrete steps saves time and increases the probability for successfully conducting the experiment when the subject's pupil is briefly aligned with the system.

With AO correction, one can create a tighter point spread function (PSF) and, consequently, can focus more light through the confocal pinhole that is placed in a retinal conjugate plane in front of the PMT. Therefore, more reflected light should reach the PMT with correction, leading to an increase in intensity in the retinal image. This effect is reflected in Fig. 3 which shows the mean intensity of the retinal image after correcting aberrations using three control methods. Despite the fact that the woofer corrected a significant amount of aberration (Fig. 2), the mean intensity of the reflectance images was typically much less than that for simultaneous and 2-step control across subjects. The mean intensity and quality of the retinal image increased considerably when adding the tweeter's correction. Simultaneous dual DM and 2-step sequential control methods yielded similar intensity values after AO correction with 2-step control providing slightly higher mean intensities across subjects.

Even though the difference in mean intensity of the retinal image between 2-step and simultaneous control was largest for subjects 4 and 5, Fig. 4 shows that the registered reflectance images were nearly identical in their appearance and spatial frequency content. Qualitatively, the reflectance images appeared nearly identical for each control method across subjects. This observation was verified by calculating and plotting the radial power spectrum for each control method in Fig. 4(c) and 4(f) for subjects 4 and 5. The power spectra resulting from 2-step and simultaneous control were very similar within each subject's eye as evidenced by the fact that their ratio was close to a value of 1 across all spatial frequencies (Fig. 5). Therefore, the direct slope-based simultaneous control algorithm is able to provide very similar image quality as the 2-step sequential control method in a shorter period of time.

#127858 - $15.00 USD Received 3 May 2010; revised 8 Jul 2010; accepted 17 Jul 2010; published 23 Jul 2010

There are additional possible benefits to using simultaneous dual DM control over 2-step sequential control. For example, one can more easily and quickly correct aberrations using simultaneous control in experimental situations when the eye's lower and higher order aberrations vary dynamically together (such as when the eye accommodates). Simultaneous dual DM control also provides the ability to optically section the retina in depth while dynamically correcting for changes in defocus and the eye's higher order aberrations concurrently. This capability could be important when imaging smaller eyes (such as rodents) in which higher order aberrations could potentially change with changes in focal plane position throughout the retina.

Finally, simultaneous dual DM control is a very flexible method which can efficiently image subjects with undilated pupils or those with incomplete Shack-Hartmann spot patterns. Figure 6 shows the Shack-Hartmann spot array and registered retinal image for a subject whose eyelid covered a portion of their dilated pupil. Consequently, it was not possible to capture a full array of Shack-Hartmann spots. However, we were still able to use this control algorithm to successfully acquire an excellent retinal image after correcting the Shack-Hartmann spots that were detected.

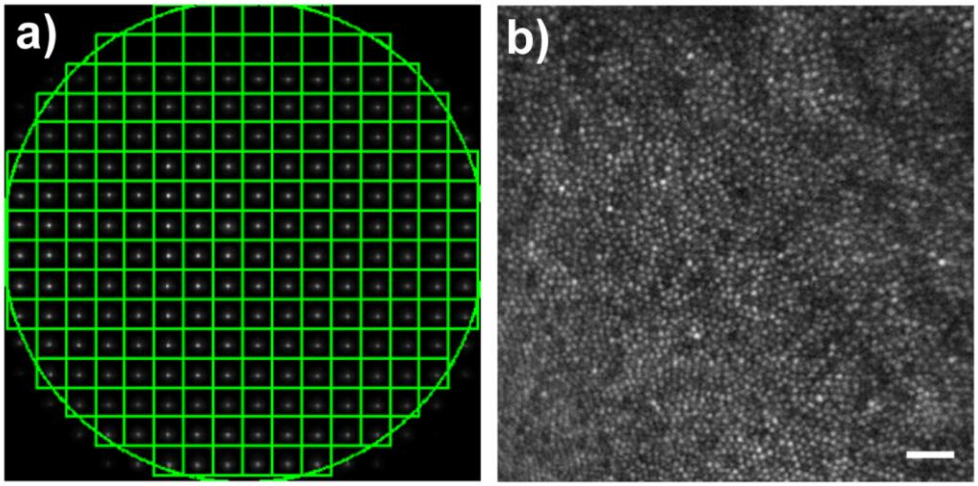

Fig. 6. (a) Shack-Hartmann spot array pattern and (b) registered reflectance image for a subject whose eyelid partially covered their dilated pupil. The top two rows of Shack-Hartmann spots were fully blocked in (a). Nevertheless, it was still possible to achieve a high quality retinal image of the cone mosaic. Registered image was taken at an eccentricity of ~1 degree and constructed from 20 frames. Scale bar represents 30 microns.

The simultaneous dual DM control method is based on the direct slope algorithm and increases system efficiency and simplicity. This method achieved a similar level of correction in normal human eyes when compared to a traditional, 2-step sequential control algorithm that used each DM independently. The simultaneous dual DM control method can be applied to any woofer-tweeter AO system (such as those used in vision science and astronomy).

Acknowledgements

This work was supported by an NIH Core Grant (P30 EY07551), the Texas Advanced Research Program under Grant No. G096152 and the University of Houston College of Optometry. The software used for single deformable mirror control of the adaptive optics system in this research was partially developed by Alfredo Dubra-Suarez, funded by a Career Award from the Burroughs Wellcome Fund, and Kamran Ahmad, funded by NIH grant BRP-EY01437 and the NSF Science and Technology Center for Adaptive Optics. We thank Ray Applegate, Stephen Burns, Don Gavel, Heidi Hofer, Wenhan Jiang, Chris Kuether, Charles Neff, Yuhua Zhang and Weiyao Zhou for their contributions and helpful discussions.

#127858 - $15.00 USD Received 3 May 2010; revised 8 Jul 2010; accepted 17 Jul 2010; published 23 Jul 2010